

Supplementary Information

The interplay between mechanics and stability of viral cages

Mercedes Hernando-Pérez, Elena Pascual, María Aznar, Alina Ionel, José R. Castón, Antoni Luque, José L. Carrascosa, David Reguera and Pedro J. de Pablo

Purification of T7 proheads

The mutant virus T7 5-am (kindly provided by Prof. F.W. Studier), containing a suppressor-sensitive mutation in the viral polymerase gene (g5), was used to produce the proheads. Cultures of the non-permissive strain BL21 E. coli were infected with this mutant phage at a multiplicity of infection of 10. Infected cultures were incubated for 45 minutes at 37°C. After the incubation no significant lysis was observed. Cells were pelleted for 10 minutes at 10,000 g. The pellet was resuspended in 5 ml TMS buffer (50 mM Tris-HCl pH 7,8; 10 mM MgCl₂; 0,1M NaCl) and treated with 200µg/ml lysozyme and 10µg/ml DNaseI for 30 minutes at 4°C. To allow membrane solubilisation samples were subsequently incubated with 10% Triton X-100 for 5 minutes at 4°C. 40 ml of 5M NaCl were finally added to the mix to induce an osmotic shock. The resultant sample was clarified by centrifugation for 20 minutes at 18,000 g. Supernatant containing the proheads was then pelleted for 1 hour 40 min at 65,000 g. Pellets were resuspended in the minimum volume of TMS buffer and centrifuged in a linear 20-40% sucrose gradient for 45 minutes at 200,000 g. Fractions containing the proheads were dialysed against TMS buffer and finally loaded in an isopycnic CsCl gradient of density 1.32 g/cm³, which was centrifuged for 14 hours at 130,000g.

Purification of empty heads of bacteriophage T7

Viral stock of infective T7 was diluted to a final concentration of 0.5 mg/ml in TMS and the ejection of DNA was induced by incubation with 2M NaClO₄ at 37°C for 16 hours. After incubation, DNase I was added up to a final concentration of 10ug/ml and allowed 1 hour digestion at room temperature. Samples were ultracentrifuged in a linear 25-50% sucrose gradient at 200,000 g for 45 minutes at 4°C. Fractions containing the tail-less empty heads were further purified by centrifugation in an isopicnic CsCl gradient of density 1.32 g/cm³ for 14 hours at 130,000g.

Coarse-Grained simulations of the indentation of T7 empty capsids

We have implemented a simulation of the indentation of a discrete model of bacteriophage T7, where the structural description is coarse-grained at the level of capsomers (the morphological units). The model considers two types of capsomers (pentamers and hexamers) that interact through an anisotropic version of a Lennard-Jones potential that incorporates the contributions of bending, the preferred curvature, and torsion¹. Pentamers only differ from hexamers in the number of neighbors and are considered to have the same effective diameter σ of hexamers. Specifically, the interaction potential is given by:

$$V(\vec{r}_{ij}, \vec{\Omega}_i, \vec{\Omega}_j) = \begin{cases} V_{LJ}(r) & r < \sigma_{LJ} \\ V_{LJ}(r)V_{ang}(\vec{r}_{ij}, \vec{\Omega}_i, \vec{\Omega}_j)V_{tot}(\vec{\Omega}_i, \vec{\Omega}_j) & r \geq \sigma_{LJ} \end{cases}$$

where the Lennard-Jones-like part of the potential

$$V_{LJ}(r) = \epsilon \left[\left(\frac{\sigma_{ij}}{r} \right)^{12} - 2 \left(\frac{\sigma_{ij}}{r} \right)^6 \right]$$

accounts for the short range steric repulsion and the longer range attraction driving the assembly of the capsid. In the previous expressions, ϵ is the binding energy between capsomers (assumed to be the same between hexamers and pentamers), r is the separation between capsomer centers and σ_{ij} their equilibrium distance, defined by the sum of the radius of the two capsomers. We take $\epsilon=20$ k_BT, a reasonable value reported in simulations²⁻⁴ with k_B being Boltzmann's constant and T the absolute temperature.

The potential is purely repulsive for $r < \sigma_{LJ}$ (being σ_{LJ} the distance at which the Lennard-Jones part of the potential is null), and the attraction for $r > \sigma_{LJ}$ is modulated by bending $V_{ang}(\vec{r}_{ij}, \vec{\Omega}_i, \vec{\Omega}_j)$ and torsion $V_{tot}(\vec{\Omega}_i, \vec{\Omega}_j)$ terms. The angular dependency of the potential is given by

$$V_{ang}(\vec{r}_{ij}, \vec{\Omega}_i, \vec{\Omega}_j) = e^{-\frac{(\theta_{ij}-v)^2}{2\alpha^2}} e^{-\frac{(\theta_{ji}-v)^2}{2\alpha^2}}$$

where θ_{ij} is the angle between vector \vec{r}_{ij} connecting capsomers i and j and vector $\vec{\Omega}_i$ which define the orientation of the capsomer (indicated by the little white sphere in Fig. 3a); v is the preferred angle of the interaction and α^2 is the inverse of the local bending stiffness. The torsion contribution is

$$V_{ang}(\vec{\Omega}_i, \vec{\Omega}_j) = e^{-k_t \frac{(1-\cos\xi)}{2}}$$

where k_t is the torsion constant and ξ the angle between the planes defined by \vec{r}_{ij} and $\vec{\Omega}_i$, and by \vec{r}_{ij} and $\vec{\Omega}_j$.

The energetically optimal configurations of this potential have been shown to reproduce successfully the same T-number structures adopted by viruses in vivo and in vitro¹. In particular, to model bacteriophage T7 we have chosen the parameters of the model that yield the optimal structure corresponding to a faceted T=7. In particular, the capsid is made of 12 pentamers (represented by red spheres) and 60 hexamers (in green) with $v = 1.796$, $\alpha = 0.7$ and $K_t = 1.5$. The results are expressed in units of ϵ (the binding energy) and σ (the diameter of the hexamers).

To mimic the set up used in the AFM experiments, we have implemented a Brownian Dynamics simulation where the coarse grained capsid is placed with the proper orientation between a flat substrate and a spherical tip of radius $R_{in}=1.5\sigma$, which has the same relative size with respect to the capsid as the tip used in the AFM experiments. The interaction between the tip and the capsomers is modeled using a purely repulsive harmonic potential with a force constant $k_c = 40 \epsilon/\sigma^2$, mimicking the cantilever's spring constant. In the simulation, the tip is initially placed at a distance h over the substrate. The simulation then runs for $3 \cdot 10^7$ time steps and the force exerted by the deformed capsid on the tip and the z-position of the tip are averaged every 104 time steps. The protocol is then repeated for different distances h , until the breakage of the capsid. The curves for the force vs. h -distance are then converted into average force vs indentation curves and the results for the different capsid orientations are plotted in Fig. 3b.

Finite Element (FE) simulations

Finite elements simulations of the AFM indentation of different models were performed using the program COMSOL Multiphysics 4.3 (Comsol, Stockholm, Sweden). In the simplest case, the capsid of bacteriophage T7 was modeled as a thick shell icosahedron of external radius $R=31.5$ nm (measured as the distance from the center to the 5-fold vertex) and thickness $h=2.5$ nm (see Fig. S2). The capsid wall was considered as made of a homogenous material with Young's modulus $E=0.4$ GPa and Poisson ratio $v=0.3$. This model capsid was oriented with the z-axis coinciding with a 5-fold, 3-fold or 2-fold symmetry axis, placed on a hard flat substrate and indented by a spherical object with radius $R_{in}=15$ nm, mimicking the AFM tip. The model was meshed with over 20000 tetrahedral elements (see Fig. S2a). The contacts between the shell and the tip as well as the supporting surface during indentation were implemented with a contact-penalty stiffness method according to the manufacturer's manual. A parametric, non-linear solver was used to simulate the stepwise lowering of the tip onto the model. The spring constant was obtained from a linear fit of the force versus indentation, for small indentations.

Fig. S3 shows the indentation curves obtained for the different orientations with a tip of $R_{in} = 15$ nm and a value of the Young's modulus of $E=0.4$ GPa chosen to reproduce values of the spring constants similar to the experimental data for empty capsids. For indentations smaller than 1.5 nm, the slopes of the indentation curves for all orientations are very similar, probably because only a normal local compression of the capsid wall is being accomplished. At

larger indentations, the order of the effective spring constants is $k_2 < k_3 < k_5$, which differs from the experimental measurements.

In order to get a better insight into the influence in the elastic response of inhomogeneities in the capsid thickness and of the real topography of bacteriophage T7, we implemented a more realistic inhomogeneous FE simulation⁵ based on the Electron Microscopy (EM) structure of bacteriophage T7 empty mature head (EMDB-1810). Starting from the EM structure, we constructed a smoothed volume model using a Gaussian filtering with a standard deviation of 1 nm. The model was then meshed uniformly with more than 10^5 tetrahedral elements (see Fig. S4a) and indented along the three different symmetry axis using the same protocol described previously. The Young's modulus and the Poisson ratio where chosen as $E = 0.2$ GPa and $\nu = 0.3$ trying to reproduce the experimental spring constants.

Fig. S5 plots the indentation curves obtained for the different orientations (5-fold, 3-fold and 2-fold). The effective spring constants k_2 and k_3 are found to be essentially identical, whereas $k_5 > k_2$. Thus, the order of the effective spring constants also differs from the experimental results.

Justification of the anisotropic stiffness based on structural information

The elastic behavior derived from continuum models of the T7 capsid is inconsistent with the AFM experiments; however, one must not forget that continuum approaches overlook the discrete nature of capsids. Recent AFM molecular simulations show that even for deep indentations the conformation of coat proteins is only slightly altered, and most part of the capsid deformation is absorbed in the junctions between subunits⁶. Additionally, the network of interactions in a viral shell is not necessarily homogeneous, and in many capsids the coat proteins form stable clusters that act as mechanical building blocks, like trimers⁷, pentamers or hexons⁸. In the case of bacteriophage T7 we identify the building blocks of the mature head from a recent cryo-EM structural study⁹. In this reference Ionel et al. show that the T7 capsid is held by polar and hydrophobic interactions, and they estimate the strength of the interactions measuring the contact surface between the different subunits (Figs S2, and S3, and. Ref⁹). Revising their results, we observe that the interaction between proteins forming pentamers and hexamers has an average contact surface of 11.4 ± 1.1 nm², which is almost four and five times higher, respectively, than the interaction observed between the coat proteins around the 3-fold axes, 3.17 ± 0.06 nm², and in the hexamer-pentamer interface, 2.3 ± 1.7 nm². This suggests that hexamers and pentamers are the mechanical building blocks of the T7 mature capsid, and the interpretation of the AFM experiments should be revised accordingly.

Hence, here we study the stiffness of the T7 capsid using the contact network of hexamers and pentamers obtained in Ref⁹. For relatively small indentations we assume that only the capsomers in direct contact with the AFM tip are displaced, and we estimate the shell stiffness calculating the total surface of the inter-capsomer contacts involved in the local deformation, which depends on the orientation of the viral capsid (see Fig. S6): five hexamer-pentamer contacts in the indentation of the 5-fold axis, $E_{5F} = 5e_{6/5}$, twelve hexamer-hexamer contacts (three internal and nine external) plus three hexamer-pentamer contacts in the 3-fold case, $E_{3F} = 12e_{6/6} + 3e_{6/5}$, and fifteen hexamer-

hexamer contacts (five internal and ten external) plus four hexamer-pentamer contacts in the 2-fold case, $E_{2F} = 15e_{6/6} + 4e_{6/5}$, where the values for the capsomer-capsomer contacts, $e_{6/6} = 3.17$ and $e_{6/5} = 4.6$, are obtained from the cryo-em reconstruction of the T7 head (Table S2 from Ref. ⁹). Since the E_{5F} , E_{3F} , and E_{2F} are expressed in surface units, we compute their ratios to estimate the relative stiffness of each axis: $E_{3F}/E_{5F} = 2.3$ and $E_{2F}/E_{5F} = 2.9$. Thus, we obtain that the 3-fold and 2-fold axes are around two and three times stiffer than the 5-fold axis, respectively. This is in very good qualitative agreement with the AFM experiments, where the indentations for the 3-fold and 2-fold axes give spring constants that are two and four times larger, respectively, than for the 5-fold case (see Table S1).

The estimation derived above is very crude, does not consider the different weight of the contacts involved in the deformation, and does not include the possible stress accumulated in the edges of the icosahedron, which could explain why in the AFM experiments the 2-fold axis is four times stiffer than the 5-fold one rather than only three times. However, despite these limitations, the contact model of capsomers gives a simple explanation of the T7 stiffness experiments, and shows the important role that the discrete nature of the shell must be playing in the mechanical response of the virus.

Supplementary Information references

1. M. Aznar and D. Reguera, *In preparation*.
2. V. S. Reddy, H. A. Giesing, R. T. Morton, A. Kumar, C. B. Post, C. L. Brooks and J. E. Johnson, *Biophys. J.*, 1998, **74**, 546-558.
3. A. Luque, R. Zandi and D. Reguera, *Proc. Natl. Acad. Sci. U. S. A.*, 2010, **107**, 5323-5328.
4. R. Zandi, D. Reguera, R. F. Bruinsma, W. M. Gelbart and J. Rudnick, *Proc. Natl. Acad. Sci. U. S. A.*, 2004, **101**, 15556-15560.
5. M. M. Gibbons and W. S. Klug, *Biophys. J.*, 2008, **95**, 3640-3649.
6. A. Arkhipov, W. H. Roos, G. J. L. Wuite and K. Schulten, *Biophys. J.*, 2009, **97**, 2061-2069.
7. I. L. Ivanovska, R. Miranda, J. L. Carrascosa, G. J. L. Wuite and C. F. Schmidt, *Proc. Natl. Acad. Sci. U. S. A.*, 2011, **108**, 12611-12616.
8. A. J. Pérez-Berná, R. Marabini, S. H. Scheres, R. Menéndez-Conejero, I. P. Dmitriev, D. T. Curiel, W. F. Mangel, S. J. Flint and C. San Martín, *J. Mol. Biol.*, 2009, **392**, 547-557.
9. A. Ionel, J. A. Velazquez-Muriel, D. Luque, A. Cuervo, J. R. Caston, J. M. Valpuesta, J. Martin-Benito and J. L. Carrascosa, *J. Biol. Chem.*, 2011, **286**, 234-242.

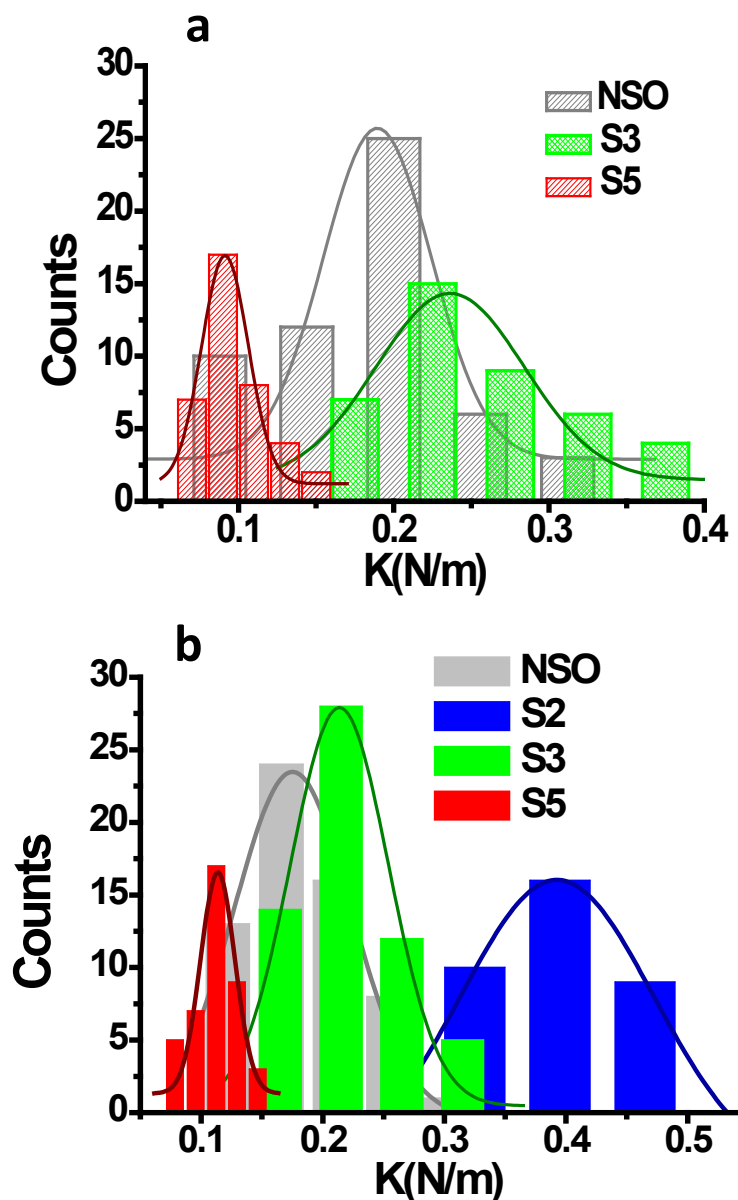


Figure S1. Histograms of particles spring constants. a) Data of proheads. b) Data of mature capsids. Blue, green and red colors correspond to particles adsorbed on 2-fold, 3-fold and 5-fold symmetry axes, respectively. Grey color depicts stiffness data from particles with no specific orientation (NSO).

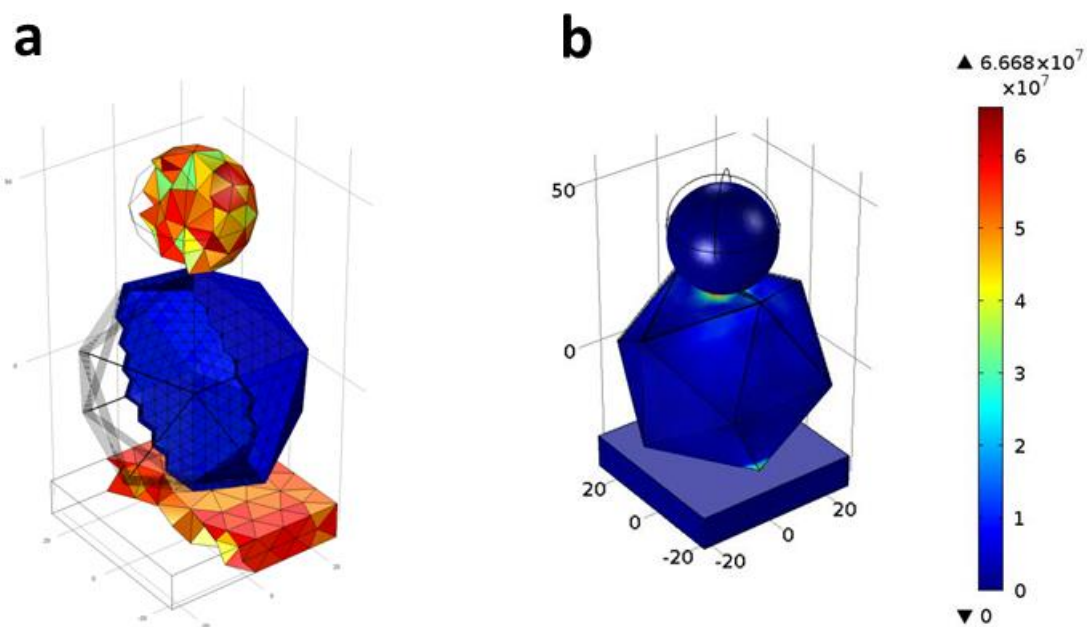


Figure S2: Geometric representation of a T7 capsid used in the FE simulations. a) The capsid is modeled as an icosahedron of external radius $R=31.5$ nm and thickness $h=2.5$ nm, and meshed with over 20000 tetrahedral elements. In this case, the capsid is oriented along its 5-fold axis. Only half of the model is shown to see the interior. b) Distribution of the von Mises stress (indicated by the color scale, in N/m^2) obtained when indenting by 3nm the icosahedron model of T7 along the 2-fold orientation.

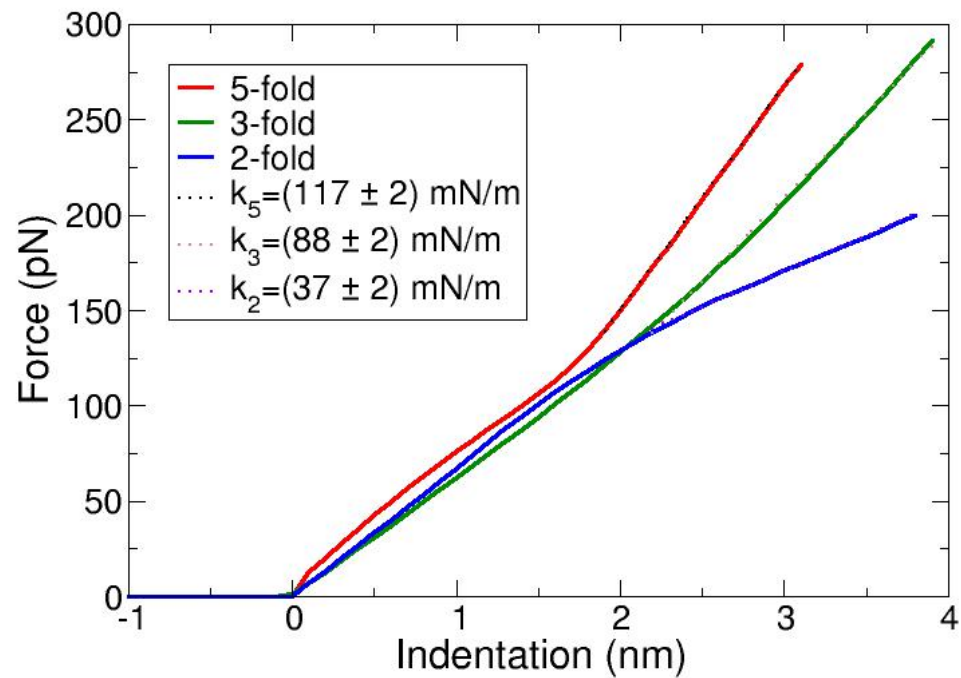


Figure S3: Indentation curves for the thick icosahedron FE T7 model. Force versus indentation curves obtained for the different orientations: 5-fold (red line), 3-fold (green line) and 2-fold (blue line) in the FE simulations of the thick icosahedron model shown in Fig. S2.

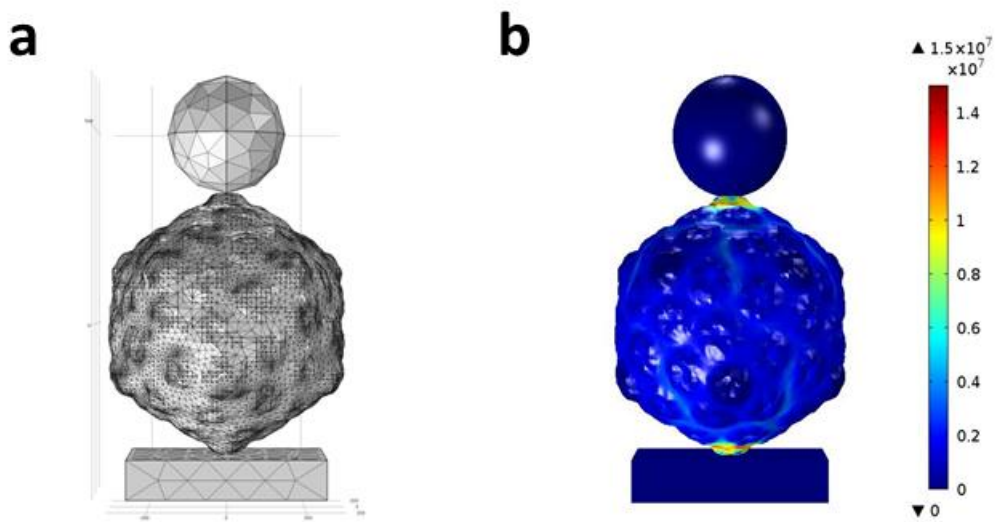


Figure S4: Inhomogeneous 3D model of a T7 capsid a) Geometric representation of the three-dimensional model of bacteriophage T7 obtained from the EM structure EMDB-1810 after a Gaussian smoothing with a standard deviation of 1nm. The structure has been meshed uniformly with more than 10^5 tetrahedral elements, and assigned a Young modulus $E=0.2$ GPa and Poisson ratio $\nu=0.3$. b) Distribution of the von Mises stress (indicated by the color scale, in N/m^2) obtained when indenting by 3nm the T7 model along the 5-fold orientation.

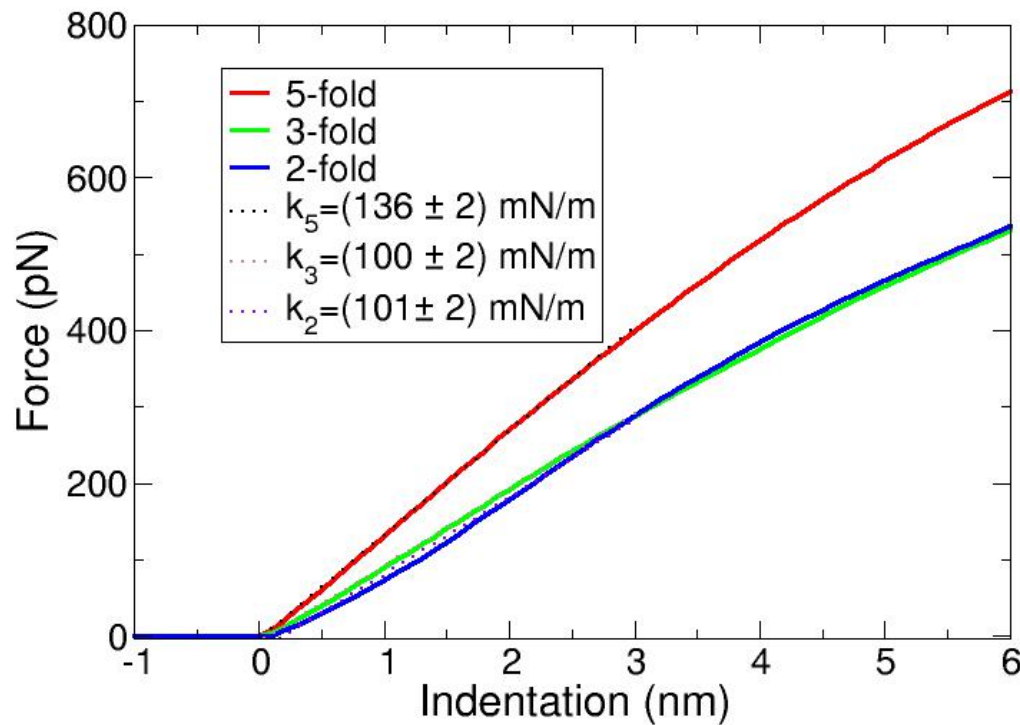


Figure S5: Indentation curves for the inhomogeneous FE T7 model. Force versus indentation curves obtained for the different orientations: 5-fold (red line), 3-fold (green line) and 2-fold (blue line) in the inhomogeneous FE simulations of the empty mature T7 capsid structure EMDB-1810 shown in Fig. S4. The dotted lines are linear fits used to get the values of the effective spring constants.

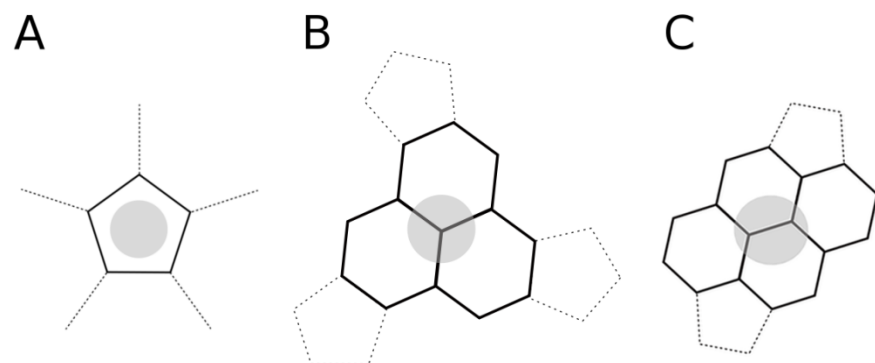


Fig. S6. Indentation environments for an icosahedral capsid. We illustrate the distribution of capsomers for the 5-fold (A), 3-fold (B), and 2-fold (C) axis of a T=7 icosahedral shell. The grey circles illustrate the contact with the AFM tip and determine the capsomers that will be displaced. The bold lines highlight the junctions that are expected to absorb most of the deformation in the indentation.

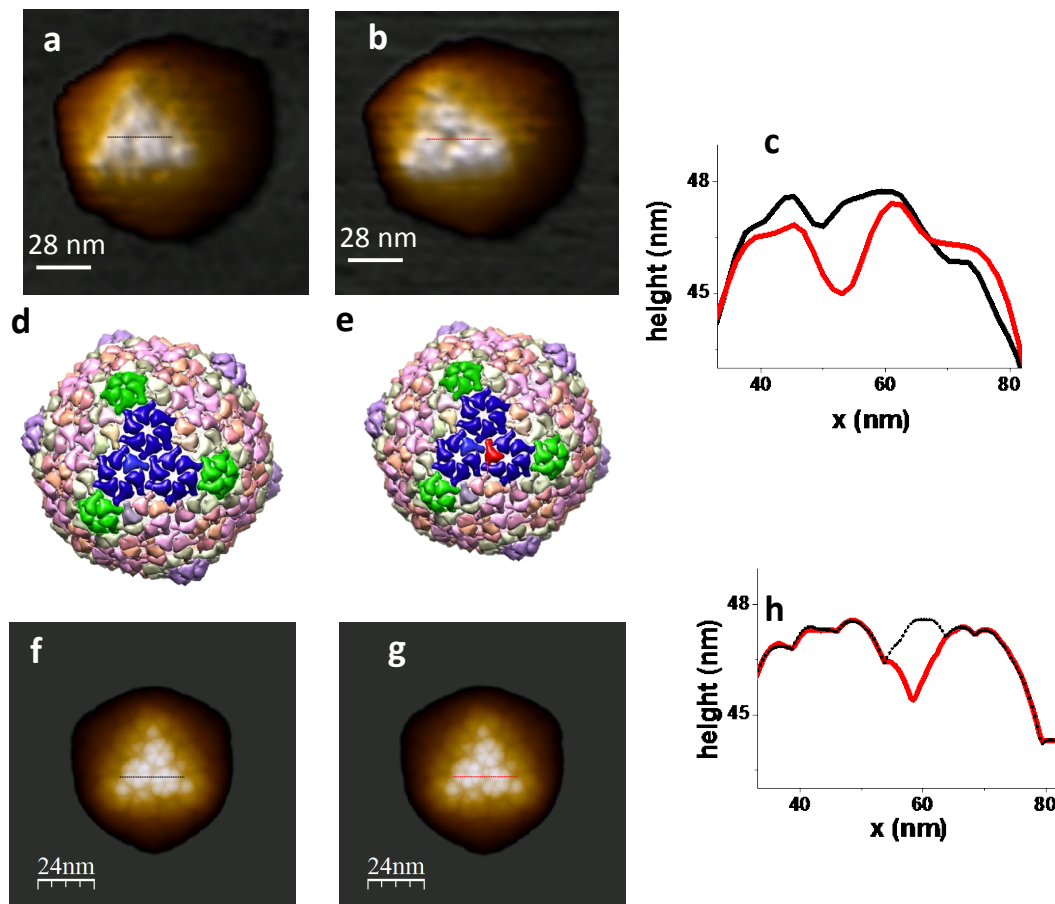


Figure S7: a) AFM topography image of a capsid before damage. b) AFM topography image of the same capsid after damage. c) Topographical profiles of the particle before (black) and after damage (red). Interpretation of the damage in the cryoEM derived model of the capsid before d) and after damage e), where the disrupted protein is depicted in red. Pentons are depicted in green and hexons in blue. f) Tip AFM-dilated model using the cryoEM volume and a 8 nm diameter tip. g) Tip AFM-dilated model where the red protein subunit of e) has been removed from the cryoEM volume. h) Topographical profiles of f) and g), where the vacant of the protein is resolved, yielding in a profile resembling the experimental data in c).

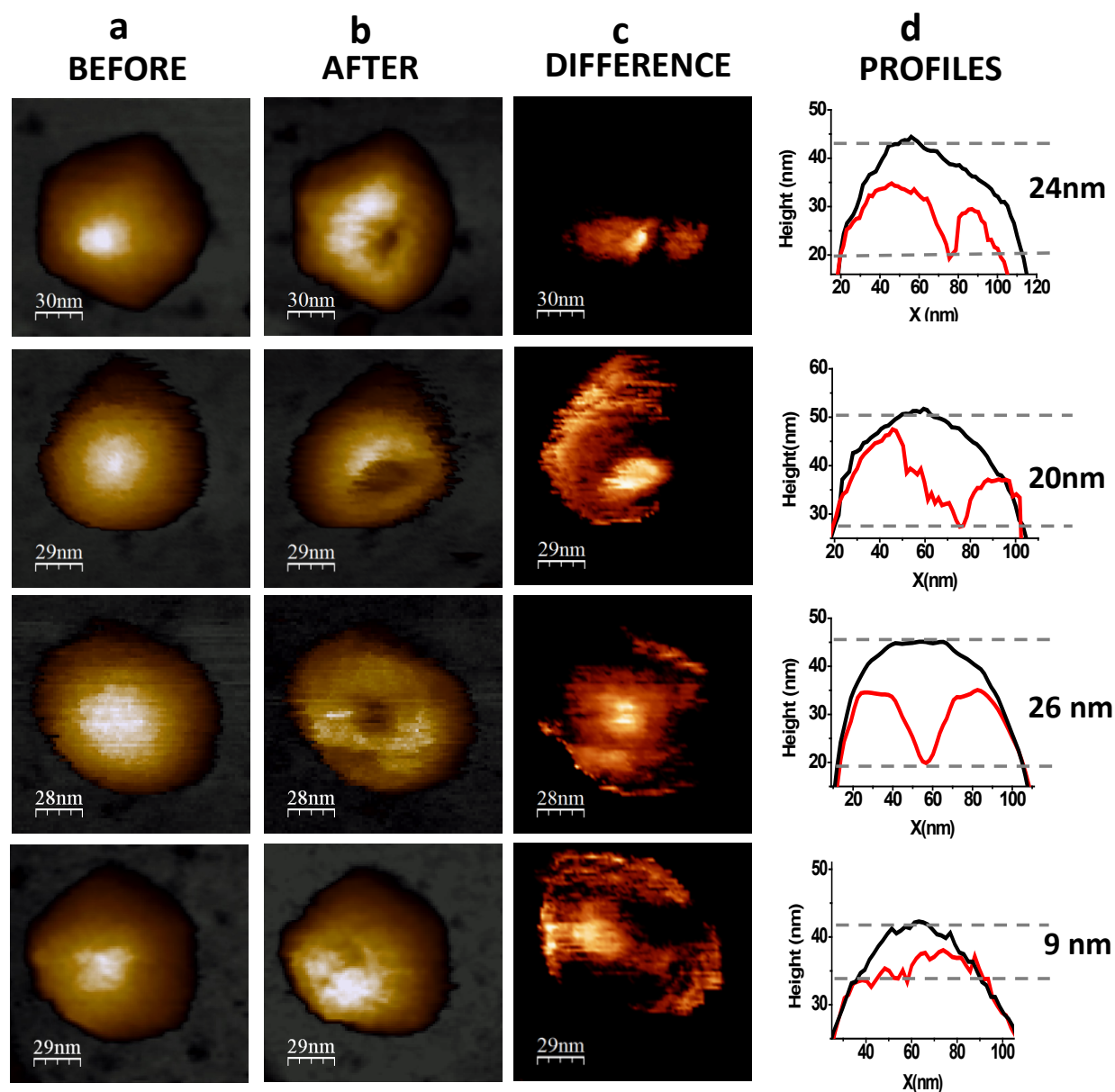


Figure S8: a) Four proheads before and b) after disruption. c) Subtraction of the topography after damage from the intact particle. d) Comparison of the profiles before (black) and after (red) damage.

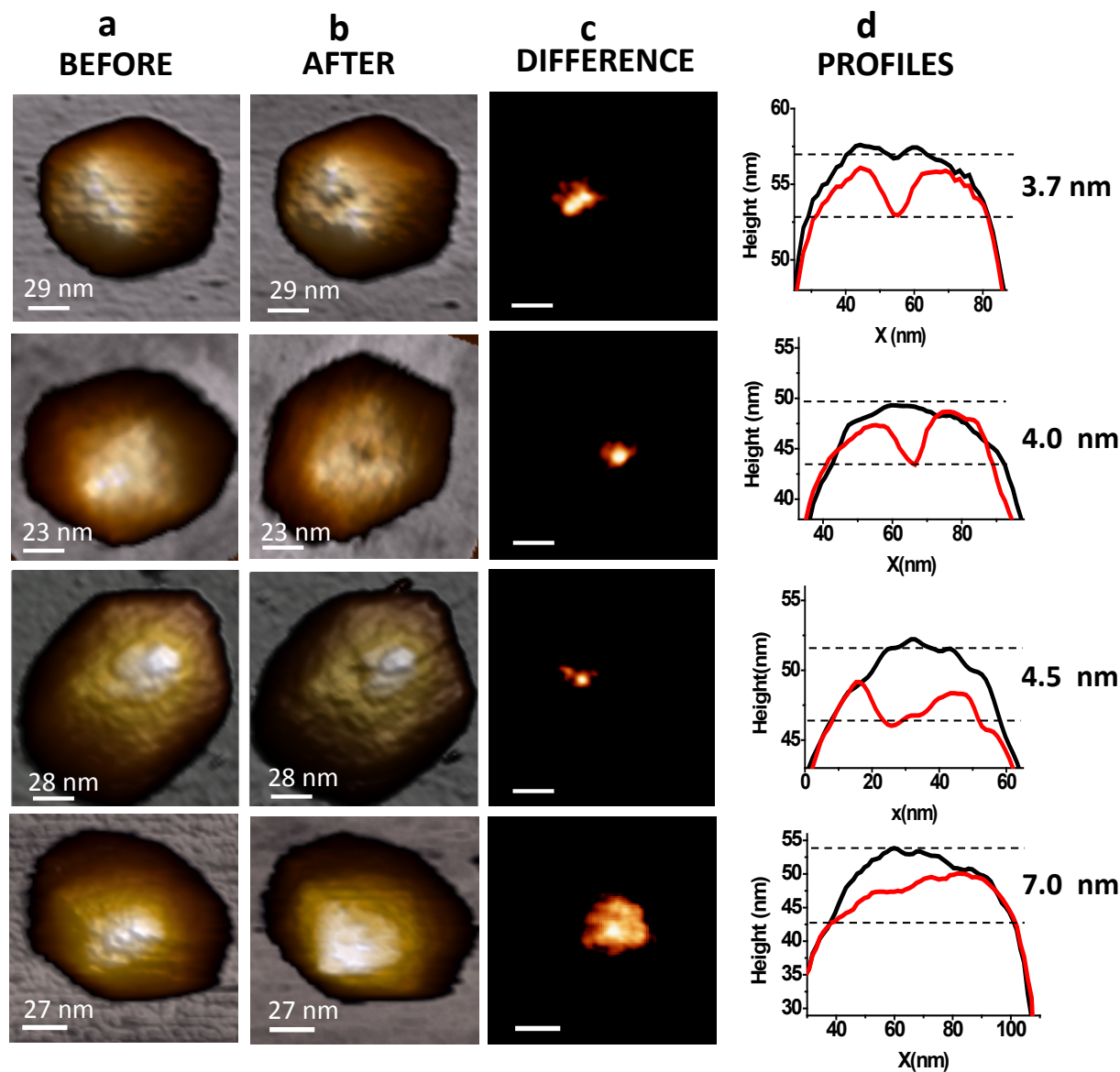


Figure S9: a) Four capsids before and b) after disruption. c) Subtraction of the topography after damage from the intact particle. d) The profiles before (black) and after (red) damage.

Table S1. T7 empty mature head relative stiffness for the different symmetries. Values of the relative stiffness derived from the AFM experiments, from the structural information, and from the coarse-grained simulations

	$k^{\text{exp}}/k^{\text{exp}}_{\text{SF}}$	E/E_{SF}	$k^{\text{CG}}/k^{\text{CG}}_{\text{SF}}$
3F/5F	1.9	2.3	1.8
2F/5F	3.6	2.9	2.3

Table S2. Geometrical data of the fractures of Fig. 6.

PARTICLE	A (nm ²)	ΔA (nm ²)	V (nm ³)	ΔV (nm ³)	ΔA/A	ΔV/V
PROHEADS	9138	2952	189644	9485	0.32305	0.05001
	9896	4989	239542	10949	0.50414	0.04571
	10966	4520	219189	12152	0.41218	0.05544
	8281	2379	177783	5318	0.28728	0.02991
	9722	4634	303041	28535	0.47665	0.09416
	11854	7944	281630	69399	0.67015	0.24642
	8161	5620	237021	32682	0.68864	0.13789
	8374	3788	220633	23230	0.45235	0.10529
CAPSID	10028	1136	287886	2127	0.11328	0.00739
	8560	205	236626	223	0.02395	9.42415E-4
	13437	1216	460000	1786	0.0905	0.00388
	9167	283.2	312458	207	0.03089	6.62489E-4
	8535	102	234128	66	0.01195	2.81897E-4
	6800	235	209313	507	0.03456	0.00242
	8779	226	226214	158.1	0.02574	6.98896E-4
	8229	441	201371	523	0.05359	0.0026
	6289	501	185831	1054	0.07966	0.00567
	7598	853	211372	1038	0.11227	0.00491